AC Polarization for Charge-Drift Elimination in Resonant Electrostatic MEMS and Oscillators

Gaurav Bahl, *Member, IEEE*, James C. Salvia, *Member, IEEE*, Renata Melamud, *Member, IEEE*, Bongsang Kim, *Member, IEEE*, Roger T. Howe, *Fellow, IEEE*, and Thomas W. Kenny, *Member, IEEE*

***Abstract*—This paper proposes the use of ac polarization for resonant electrostatic microelectromechanical systems that eliminates the frequency drift caused by dielectric charging and charge screening. It is mathematically and experimentally shown that an ac-polarized resonator can sustain stable oscillations when used in a positive feedback oscillator circuit. We also demonstrate an oscillator topology that generates a drift-free reference frequency tone with this technique in spite of using a resonator that exhibits large frequency drifts under dc polarization. Long-term data are presented for these drift-susceptible devices, showing a significant improvement in frequency stability. [2010-0104]**

***Index Terms*—AC biasing, charging, dielectrics, drift, frequency stability, oscillators, resonators.**

I. Introduction

DIELECTRICS play an important role in many classes of microelectromechanical systems (MEMS). They are frequently used for electrical isolation, as structural elements [1], [2], for enhancing the transduction within electrostatic actuators [3], [4], and, more generally, as sacrificial layers. However, it is also well known that dielectrics are susceptible to various charging phenomena. Charge buildup and charge motion can screen electrode potentials, affecting the overall electromechanical properties of the device [5]–[8]. In some devices, the actuation method itself is susceptible to charging, such as in capacitive shunt RF switches [9]. Occasionally, charged particles may be involved in the experiment, such as in fluid environments and ionic solutions [10]–[12]. Additionally, it may not be possible to guarantee a hermetic packaging environment, and contamination and humidity can also introduce detrimental charge. Since charging is not always avoidable, techniques that can circumvent the undesirable effects of charge (for instance, [11], [13], and [14]) can be of value.

Recently, SiO_2-coated silicon micromechanical resonators have been shown to possess very desirable frequency-versus-temperature characteristics due to the oxide-facilitated passive compensation of stiffness [15]. This improved temperature performance makes them very useful for frequency reference applications. However, it has also been noted that these SiO_2 coatings are susceptible to charging [5]. Variations in the charge state cause the resonance frequency to drift with time. Motional impedance can also change as the charge varies and screens the polarization voltage.

In this paper, we present a technique in which ac polarization of the resonator can be used to circumvent charge drifts. We mathematically discuss how a resonator responds under ac polarization and how an oscillator functions under such a scheme of operation. Experimental data are also presented to support the theoretical arguments. We propose a practical frequency reference using this methodology. Finally, we present long-term frequency-stability observations of a drift-prone device, showing the elimination of the charge drifts, thus demonstrating the effectiveness of this ac polarization methodology.

II. Sinusoidal AC Polarization

We have previously reported time constants associated with drifts of frequency in the SiO_2-coated microresonators that are on the order of tens to thousands of seconds. These drifts vary with temperature and biasing conditions [5]. Since our previous reasoning suggests that the charge moves due to the force experienced under the applied dc electric field, reversing the electric field polarity should reverse the force and the drift. Consequently, the use of a sinusoidal ac-only (zero dc) polarization source that causes electric fields within the system to reverse at a regular rate, at a 50% duty cycle, has been proposed [14]. This method should prevent any net motion of the charge by balancing forces experienced in either direction. In addition, if the field reversal takes place at a rate that is much faster than the time constants associated with charging behavior, one can expect significant attenuation of the motion of charge. As long as there is no preference of charge motion toward either field polarity, the charge will effectively cease to "move."

Manuscript received April 13, 2010; revised October 5, 2010; accepted November 1, 2010. This work was supported in part by the Defense Advanced Research Projects Agency (DARPA) under Grant HR0011-06-0049 (Dr. D. L. Polla, Program Manager), by Bosch, by Epson, by HP, by Agilent, by Boeing, by Qualcomm, by the DARPA Harsh Environment Robust Micromechanical Technology under Grant ONR N66001-03-1-8942, by the National Nanofabrication Users Network facilities funded by the National Science Foundation under Award ECS-9731294, and by the National Science Foundation Instrumentation for Materials Research Program under Grant DMR 9504099. The work of J. C. Salvia was supported in part by a National Science Foundation Graduate Fellowship. The work of R. Melamud was supported in part by a Stanford Graduate Fellowship. Subject Editor C. Hierold.

G. Bahl is with the Electrical Engineering and Computer Science Department, University of Michigan, Ann Arbor, MI 48109-2122 USA (e-mail: bahlg@umich.edu).

J. C. Salvia and R. Melamud are with SiTime Corporation, Sunnyvale, CA 94085 USA (e-mail: jsalvia@stanford.edu; rmelamud@gmail.com).

B. Kim is with Sandia National Laboratories, Alberquerque, NM 87185-1194 USA (e-mail: bongsang@gmail.com).

R. T. Howe is with the Electrical Engineering Department, Stanford University, Stanford, CA 94305-9505 USA (e-mail: rthowe@stanford.edu).

T. W. Kenny is with the Mechanical Engineering Department, Stanford University, Stanford, CA 94305-3030 USA (e-mail: tkenny@stanford.edu).

Color versions of one or more of the figures in this paper are available online at http://ieeexplore.ieee.org.

Digital Object Identifier 10.1109/JMEMS.2010.2100027

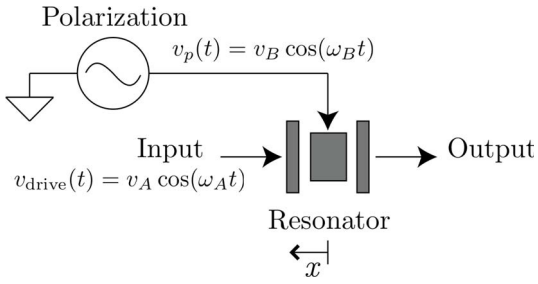

Fig. 1. Schematic for open-loop ac-only probing of an electrostatic resonator. The polarization source is at a fixed frequency ω_B. When this frequency $\omega_B = 0$, this source becomes a dc voltage v_B. As a result, the mathematics discussed in this paper can be specialized for dc sources that we are already familiar with. The positive direction for x is defined.

A similar technique is applied in RF switches, where bipolar actuation can reduce charging and extend the lifetime of the devices [13]. In the context of resonators, a local oscillator is occasionally used to observe resonance in the presence of a large feedthrough, although this method also incorporates a dc potential source to reduce the motional impedance of the device [16]. The nonlinear technique of driving at half the resonator's frequency also requires dc to extract the motion signal from the device [17].

Since the polarization voltage $v_p(t)$ is being modulated sinusoidally, it is reasonable to expect associated changes in the spring constant due to the electrostatic spring-softening effect. However, since the frequency of this modulation is far below the bandwidth of the oscillator circuitry as well as the resonance frequency of the device, the spring constant of the resonator can be treated as a quasi-static value for any short instant of time. We will discuss the modulation of this spring constant in Section IV-D.

III. Open-Loop Response

To test the open-loop response, the resonator is biased with a sinusoidal polarization source at frequency ω_B and excited with another ac signal at frequency ω_A (see Fig. 1). In this open-loop configuration, the admittance spectrum of the device shows two resonances (see Fig. 2). These electrical resonances occur at frequencies $\omega_{\text{Res}} - \omega_B$ and $\omega_{\text{Res}} + \omega_B$, where ω_{Res} is the peak mechanical resonance frequency of the device. It is useful to mathematically step through the processes that give rise to such open-loop behavior in order to explain the multifrequency closed-loop operation in an oscillator.

A. Resonator Drive

The electrostatic force for a single parallel-plate capacitor, when a voltage V is applied across it, is known to be

$$F = \frac{\epsilon A V^2}{2g^2} \tag{1}$$

where A is the transduction area, g is the transduction gap of the capacitor, and ϵ is the equivalent permittivity of the dielectrics between the capacitor plates. For a two-capacitor system (see Fig. 1), assuming that both input and output

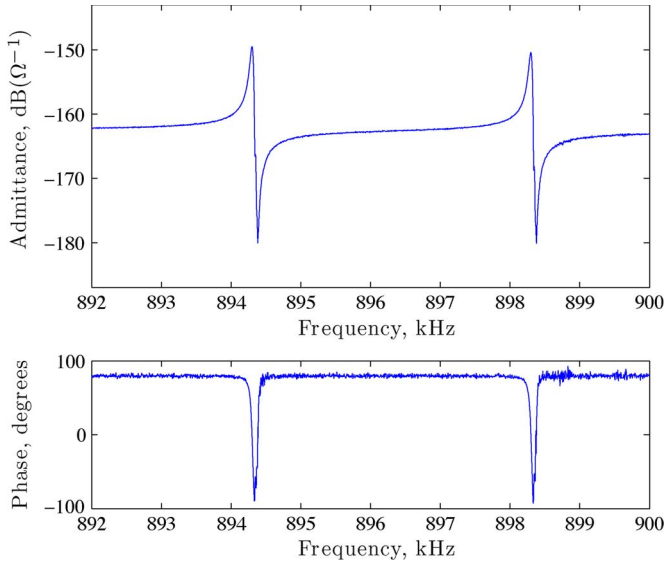

Fig. 2. Resonator electrical admittance magnitude and phase under ac polarization, observed through a network analyzer, for a $\omega_{\text{Res}} \approx 2\pi \times 896$ krad/s (896 kHz) silicon-only resonator. Here, $\omega_B = 2\pi \times 2$ krad/s (2 kHz), and the resonance peaks appear around 894 and 898 kHz. The location of these peaks depends on ω_B, and they are identified as $\omega_{\text{Res}} - \omega_B$ and $\omega_{\text{Res}} + \omega_B$.

electrodes are nominally grounded, the drive force equation is given by

$$F(t) = \frac{\epsilon A}{2(g-x)^2}\left(v_p(t) - v_{\text{drive}}(t)\right)^2 - \frac{\epsilon A}{2(g+x)^2} v_p^2(t) \tag{2}$$

assuming a displacement x applied to the device (the direction defined in Fig. 1). When x is small compared to g and the polarization and drive are sinusoids

$$v_p(t) = v_B \cos(\omega_B t) \tag{3}$$

$$v_{\text{drive}}(t) = v_A \cos(\omega_A t) \tag{4}$$

the force equation (2) can be simplified to

$$F(t) = \kappa \frac{v_A^2}{2} + \kappa \frac{v_A^2}{2} \cos(2\omega_A t) - \kappa v_A v_B \left[\cos\left((\omega_A - \omega_B)t\right) + \cos\left((\omega_A + \omega_B)t\right)\right] \tag{5}$$

where

$$\kappa = \frac{\epsilon A}{2g^2}. \tag{6}$$

This force function can drive the resonator effectively when one of the following is true:

$$\begin{aligned} \omega_A - \omega_B &\approx \omega_{\text{Res}} \\ \omega_A + \omega_B &\approx \omega_{\text{Res}} \\ 2\omega_A &\approx \omega_{\text{Res}}. \end{aligned} \tag{7}$$

In (5) and (7), the terms with $2\omega_A \approx \omega_{\text{Res}}$ are unlikely to drive the resonator efficiently since the corresponding force amplitude is typically very low $(v_A \ll v_B)$ compared to the rest of the terms. One can, however, expect the resonator

to show small motional impedance when $\omega_A = \omega_R - \omega_B$ or when $\omega_A = \omega_R + \omega_B$, where $\omega_R \approx \omega_{\rm Res}$ is a frequency near the mechanical resonance peak. As a result, the drive force expression can be simplified to

$$F(t) = -\kappa v_A v_B \left[\cos\left((\omega_A - \omega_B)t\right) + \cos\left((\omega_A + \omega_B)t\right)\right]. \tag{8}$$

The variables ω_1 and ω_2 can also be introduced as

$$\begin{aligned} \omega_1 &= \omega_R - \omega_B \\ \omega_2 &= \omega_R + \omega_B. \end{aligned} \tag{9}$$

Since the resonator can be approximated as a linear time-invariant device, one can model its force-displacement response as a high-Q transfer function $H_F(\omega)$, which filters out force components away from resonance. If either $\omega_A = \omega_1$ or $\omega_A = \omega_2$ and ω_B is much larger than the resonator bandwidth, only one of the two cosines in (8) will lie close to $\omega_{\rm Res}$. In that case, one of the two cosines can be dropped in the analysis, depending on the chosen drive frequency ω_A. The result is a force at frequency ω_R in either case, and the simplified forcing function can be written as

$$F(t) = -\kappa v_A v_B \cos(\omega_R t). \tag{10}$$

Note that, in the dc polarization case ($\omega_B = 0$), the two cosines in (8) coincide, and the driving force has a double magnitude. In the ac polarization case, however, the simplified motion response is represented as

$$x(t) = -\kappa v_A v_B H_R \cos(\omega_R t + \phi_R) \tag{11}$$

where $H_F(\omega)$ is modeled as a magnitude H_R and phase ϕ_R modification to the input cosine. It is important to note that, close to resonance, $\phi_R \approx -\pi/2$. At resonance, $H_R = Q/k$, where Q is the quality factor and k is the spring constant for the resonator.

B. Output Current Generation

Due to motion $x(t)$, the output capacitor varies as a function of time $C(t)$. Subsequently, $C(t)$ can be linearized with a Taylor expansion and represented in the form

$$C(t) = C_o\left(1 - \frac{x(t)}{g}\right) \tag{12}$$

where $C_o = \epsilon A/g$ is the zero-displacement capacitance of the output transducer. This motion mixes with $v_p(t)$ again in the output capacitor and generates output electrical currents through

$$i(t) = v_p(t)\frac{dC(t)}{dt} + C(t)\frac{dv_p(t)}{dt}. \tag{13}$$

Here, it is noted that the second term in (13) does not appear when the polarization is dc only. In general, the following three output currents appear:

$$\begin{aligned} i_1(t) &= -v_A\gamma\cdot(\omega_R - \omega_B)\cdot\sin\left((\omega_R - \omega_B)t + \phi_R\right) \\ i_2(t) &= -v_A\gamma\cdot(\omega_R + \omega_B)\cdot\sin\left((\omega_R + \omega_B)t + \phi_R\right) \\ i_{\rm feedthrough}(t) &= -\omega_B C_o v_B \sin(\omega_B t) \end{aligned} \tag{14}$$

where

$$\gamma = \frac{\kappa v_B^2 C_o H_R}{2g} = \frac{\epsilon^2 A^2 v_B^2 H_R}{4g^4}. \tag{15}$$

The feedthrough term in (14) may be ignored since it is not seen to participate in oscillations and is possible to electrically filter since, usually, $\omega_B \ll \omega_R$. Additionally, one can rewrite

$$i_{\rm out}(t) = i_1(t) + i_2(t) \tag{16}$$

where

$$\begin{aligned} i_1(t) &= -\omega_1 v_A \gamma \cdot \sin(\omega_1 t + \phi_R) \\ &= \omega_1 v_A \gamma \cdot \cos(\omega_1 t + \phi_R + \pi/2) \\ i_2(t) &= -\omega_2 v_A \gamma \cdot \sin(\omega_2 t + \phi_R) \\ &= \omega_2 v_A \gamma \cdot \cos(\omega_2 t + \phi_R + \pi/2). \end{aligned} \tag{17}$$

Here, it is noted that both output currents $i_1(t)$ and $i_2(t)$ will be generated even though the voltage excitation $v_{\rm drive}(t)$ is only at one frequency in (4), i.e., $\omega_A = \omega_1$ or ω_2. When the frequency $\omega_B = 0$, i.e., the polarization is dc only, then the two currents i_1 and i_2 merge into one, and the feedthrough term in (14) disappears.

C. Network Analyzer Measurement

It is interesting to note that the output currents are scaled with their respective frequency. As mentioned previously, output currents appear at both frequencies ω_1 and ω_2 irrespective of whether the drive signal frequency ω_A is at ω_1 or at ω_2. However, since the network analyzer source only generates a drive voltage at one frequency at a time and senses the output from the device at the same frequency using a lock-in method, the second output current is not observable in this manner of open-loop probing. As a result, when one attempts to observe the voltage-to-current transfer function, one notes different values of resonator impedance at each resonance. The apparent resistance at frequency ω_1 is greater than that at ω_2 due to this scaling of currents in equation set (17).

We can evaluate the apparent motional resistances at resonance ($\omega_R = \omega_{\rm Res}$), noting that, at resonance, the value of ϕ_R should be $-\pi/2$

$$\begin{aligned} R_1 &= \frac{v_A}{i_1} = \frac{1}{\gamma\omega_1}\bigg|_{\omega_R = \omega_{\rm Res}} = \frac{1}{(\omega_{\rm Res} - \omega_B)}\frac{4g^4}{\epsilon^2 A^2 v_B^2 H_R} \\ R_2 &= \frac{v_A}{i_2} = \frac{1}{\gamma\omega_2}\bigg|_{\omega_R = \omega_{\rm Res}} = \frac{1}{(\omega_{\rm Res} + \omega_B)}\frac{4g^4}{\epsilon^2 A^2 v_B^2 H_R}. \end{aligned} \tag{18}$$

Under dc polarization, the motional resistance takes on the value

$$R_{\rm dc} = \frac{v_A}{i_{\rm out,dc}} = \frac{1}{4\gamma\,\omega_{\rm Res}} = \frac{1}{\omega_{\rm Res}}\frac{g^4}{\epsilon^2 A^2 v_B^2 H_R} \tag{19}$$

which is four times smaller than the motional resistance observed from the ac polarization peaks (at $\omega_B = 0$) for the same value of v_B. This notable change occurs due to two effects:

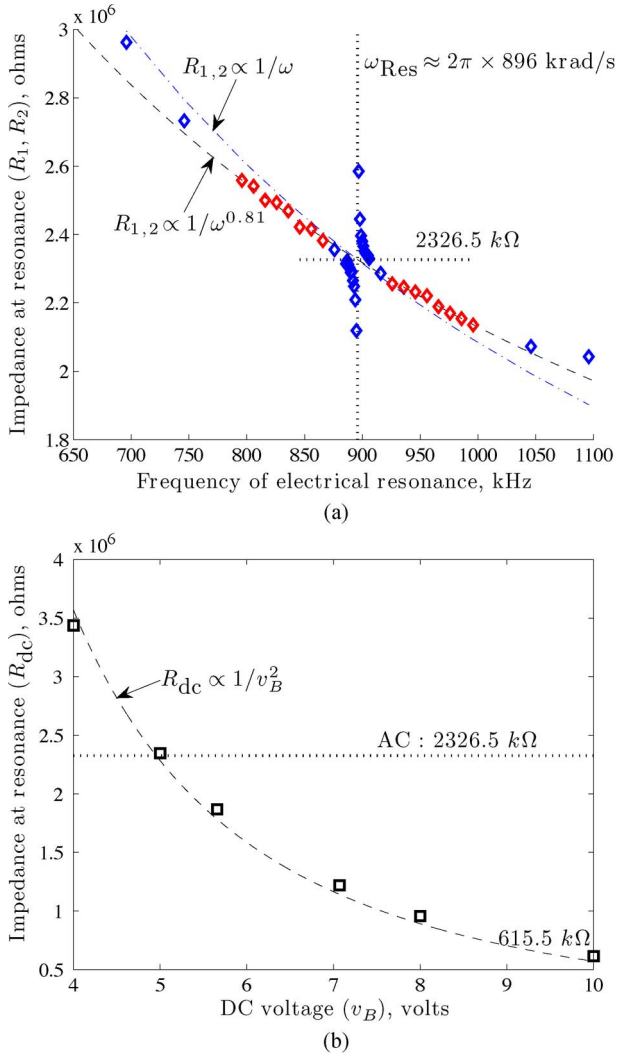

Fig. 3. Comparison of observed electrical impedance in ac and dc polarization cases. (a) Mapping open-loop motional resistance of upper (R_2, greater than 896 kHz) and lower (R_1, less than 896 kHz) sidebands with ac polarization against the respective resonance frequencies, as a function of changing ω_B from 1 to 200 kHz, at fixed amplitude $v_B = 10$ V. The presented curve fits (using red data points) are extrapolated to $\omega_B = 0$ to compare against the dc case in (b). (b) Mapping open-loop motional resistance of dc resonance as a function of changing v_B. Theoretically, the experimentally obtained 2.32-MΩ value for $v_B = 10$ V ac polarization should intersect the dc curve at $v_B = 5$ V. This is also experimentally seen.

1) The drive force in the ac polarization case is scaled by 1/2 compared to that of the dc polarization case, as mentioned previously with (10), and 2) the output current is further split between the two sidebands, as shown in (14).

Fig. 3(a) shows the observed values of the motional resistance at the resonance peak for each R_1 and R_2 pair in the form of a combined variable $R_{1,2}$. Measurements were taken for ω_B from 1 to 200 kHz, with $v_B = 10$ V. A curve fit to the relation $R_{1,2} \propto 1/\omega$ is shown, originating from the theoretical result of equation set (18). However, it was determined via curve fitting that $R_{1,2} \propto 1/\omega^{0.81}$ better indicates the data trend. The reason for this discrepancy is not understood.

As the two electrical resonances converge for small ω_B, the apparent motional resistances diverge from the aforementioned theory. This is because ω_B is now comparable to the resonance bandwidth, and the assumption used to obtain (10) is no longer valid. The drive force from both cosine terms in (8) now contributes to the motion of the device and to the observed $i_{\rm out}$ at the frequency being probed by the analyzer. In the limiting case ($\omega_B \to 0$), only one electrical resonance exists. This is experimentally seen as the upper sideband diminishes, i.e., its motional resistance R_2 rises, while the lower sideband motional resistance R_1 drops toward the dc polarization value $R_{\rm dc}$ for the v_B chosen.

Fig. 3(b) shows the measured motional resistance for various values of dc voltage v_B. We see that the theoretical prediction of 1 : 4 scaling of the resistance between the ac and dc cases with the same v_B is fairly good (at $v_B = 10$ V). Additionally, one can predict from the aforementioned equations that $R_{\rm dc} = R_{1,2}$ when $v_B|_{\rm dc} = (1/2)v_B|_{\rm ac}$. This is also observed at the $v_B = 5$ V mark.

IV. Closed-Loop Oscillator

A. Signal Circulation

We start this set of arguments from the force function $F(t)$ in (10) which we assume to be generated through some as yet unknown drive voltage waveform in the oscillator system. We will close the loop on this force function, enforcing positive feedback, and determine the relationships between the signals. As shown in the previous section, this force $F(t)$ yields motion $x(t)$, subsequently generating output currents $i_{\rm out}(t)$ in (16). This time, the output currents $i_{\rm out}(t)$ are passed through a transimpedance amplification circuit with some appropriate gain and phase response. Due to linearity and time invariance of the circuit, one obtains voltage signals at the same two frequencies as those present in the output current (17), with magnitude (v_1, v_2) and phase (ϕ_1, ϕ_2), which can be modeled on the specific electrical systems in use

$$v_{\rm drive}(t) = v_1 \cos(\omega_1 t + \phi_1) + v_2 \cos(\omega_2 t + \phi_2). \qquad (20)$$

We reuse the variable $v_{\rm drive}(t)$ since the output of the amplifier is applied back to the drive electrode in a closed-loop operation. To be more specific

$$\begin{aligned} \phi_1 &= \phi_R + \pi/2 + \phi_{c1} \\ \phi_2 &= \phi_R + \pi/2 + \phi_{c2} \end{aligned} \qquad (21)$$

where ϕ_{c1} and ϕ_{c2} are the phases added by the circuit at each of the two frequencies. The exact values for v_1 and v_2 are set by a variable gain element within the circuit and are thus determined during the loop operation.

Generalizing the summarized forcing function from (8), the following drive force $F(t)$ is obtained for the $v_{\rm drive}(t)$ in (20):

$$\begin{aligned} F(t) = &-\kappa v_1 v_B [\cos((\omega_1 - \omega_B)t + \phi_1) + \cos((\omega_1 + \omega_B)t + \phi_1)] \\ &- \kappa v_2 v_B [\cos((\omega_2 - \omega_B)t + \phi_2) + \cos((\omega_2 + \omega_B)t + \phi_2)]. \end{aligned} \qquad (22)$$

The cross-mixing components of the two cosines within $v_{\rm drive}(t)$ are also ignored in this since they do not have sufficient

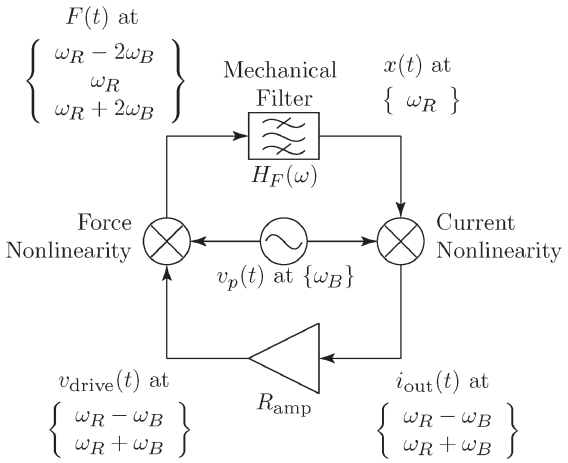

Fig. 4. Visualization aid for simplified oscillator signals. The signals and their respective dominant frequency components are indicated. The two mixer blocks do not function as real mixers in this diagram but only indicate frequency intermodulation from the inputs to the outputs. Note that, although there are two dominant electrical frequencies $\omega_R \pm \omega_B$, only one dominant mechanical frequency ω_R exists in the system.

amplitude to cause actuation. Replacing the values of ω_1 and ω_2 into the aforementioned expression yields

$$F(t) = -\kappa v_1 v_B \left[\cos\left((\omega_R - 2\omega_B)t + \phi_1\right) + \cos(\omega_R t + \phi_1)\right] - \kappa v_2 v_B \left[\cos(\omega_R t + \phi_2) + \cos\left((\omega_R + 2\omega_B)t + \phi_2\right)\right]. \tag{23}$$

Only the ω_R terms in the aforementioned expression lie within the resonator bandwidth. The other two terms $(\omega_R \pm 2\omega_B)$ can be placed outside the resonance response band with a suitable choice of ω_B. As a result, the drive force is generated at the same frequency ω_R that we began the closed-loop arguments with, thus completing the loop. A visualization aid is presented in Fig. 4 showing the interaction between various frequencies within the system. With this figure, we can see how the electrostatic transduction nonlinearities cause heterodyning, i.e., frequency mixing, of the signals around the loop.

We have successfully tested several ac-polarized devices with oscillators (circuit design previously discussed in [18]), and we have experimentally observed behavior consistent with the aforementioned simplified theory. A representative result is shown in Figs. 5 and 6 where a silicon-only (hence, drift-free) resonator with an 896-kHz resonance frequency was employed to produce oscillations under a 10-kHz polarization frequency.

B. Oscillator Phase Condition

For successful oscillation, the resulting force $F(t)$ in (23) must be of identical magnitude and be in phase with the originating force in (10), i.e., the loop gain is exactly one. A simplified forcing function can be constructed from (23) to yield

$$F(t) = -\kappa v_B (v_1 \cos\phi_1 + v_2 \cos\phi_2) \cdot \cos(\omega_R t) + \kappa v_B (v_1 \sin\phi_1 + v_2 \sin\phi_2) \cdot \sin(\omega_R t). \tag{24}$$

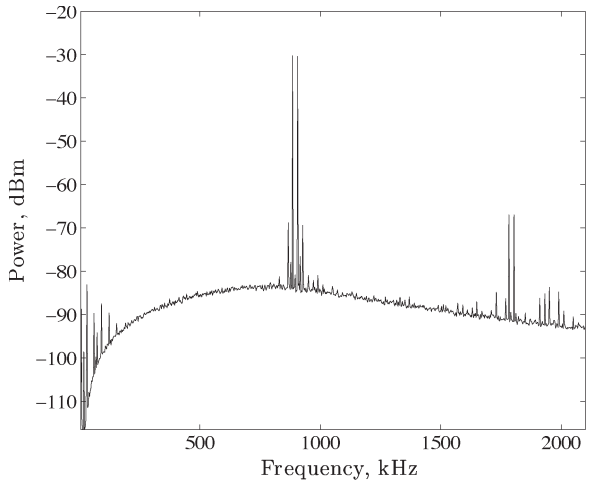

Fig. 5. Oscillator output spectrum for a silicon-only resonator with $\omega_{\rm Res} \approx 2\pi \times 896$ krad/s (896 kHz) with $\omega_B = 2\pi \times 10$ krad/s (10 kHz). Data were acquired with a 30-Hz bandwidth. The dominant dual electrical oscillation peaks $\omega_R \pm \omega_B$ are visible near 896 kHz. In addition, we see low-frequency noise appearing from harmonics of the polarization signal and nearby noise sources. The harmonics of the dual oscillation peaks are also apparent around 1800 kHz.

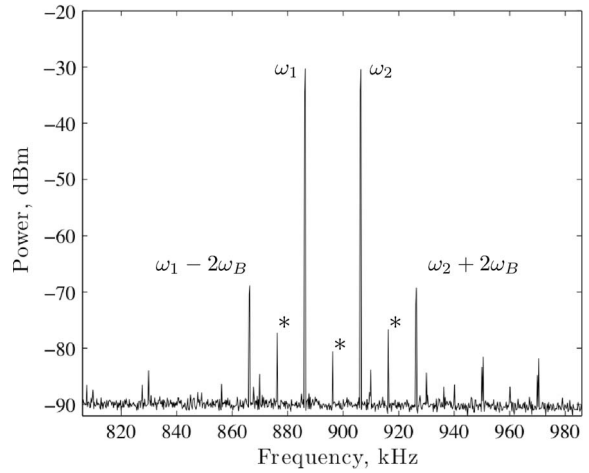

Fig. 6. Close-up view of the oscillator output spectrum shown in Fig. 5. These data were acquired with a 10-Hz bandwidth. The dual electrical oscillation peaks are visible at $\omega_1 = \omega_R - \omega_B$ and $\omega_2 = \omega_R + \omega_B$, and AM and FM artifacts are visible at $\omega_1 - 2\omega_B$ and $\omega_2 + 2\omega_B$. Additional spurs are also apparent at ω_B intervals (peaks marked with $*$), which are likely due to intermodulation of the various signals present in the system. The sources of most of the smaller unidentified spurs in this spectrum are unknown.

This can be rewritten as

$$F(t) \propto \cos(\omega_R t + \phi_{\rm FB}) \tag{25}$$

where the feedback phase is

$$\phi_{\rm FB} = \tan^{-1}\left(\frac{v_1 \sin\phi_1 + v_2 \sin\phi_2}{v_1 \cos\phi_1 + v_2 \cos\phi_2}\right). \tag{26}$$

Since the original force in (10) had a zero phase, we must impose the condition $\phi_{\rm FB} = 0$ for positive feedback. Thus, the following relation is obtained:

$$v_1 \sin\phi_1 + v_2 \sin\phi_2 = 0. \tag{27}$$

The expressions for ϕ_1 and ϕ_2 can be substituted from equation set (21). Here, since the phase shifts ϕ_{c1} and ϕ_{c2} are fixed by the circuit, the resonator must adjust its phase ϕ_R to satisfy this overall phase condition. With some manipulation of (27), the following phase solution can be obtained:

$$\phi_R = -\frac{\pi}{2} - \tan^{-1}\left(\frac{v_1 \sin\phi_{c1} + v_2 \sin\phi_{c2}}{v_1 \cos\phi_{c1} + v_2 \cos\phi_{c2}}\right). \tag{28}$$

It is concluded that the oscillator phase shift determines the operating point of the resonator. The one-to-one phase–frequency relationship of the resonator then helps determine the operating frequency ω_R of the loop. Subsequently, the amplitude–frequency relationship determines the motional impedance of the device seen by the circuit. The gain controller within the circuit then determines and sets the appropriate gain to determine the values of v_1 and v_2 for a loop gain of one.

Although it is not necessary to attain the lowest motional impedance of the device, it is best to operate near the resonance peaks, where one expects that $\phi_R \approx -\pi/2$. This implies that the phase shifts from the circuit ϕ_{c1} and ϕ_{c2} must be small. Making this small-angle assumption, (28) can be simplified to

$$\phi_R = -\frac{\pi}{2} - \frac{v_1\phi_{c1} + v_2\phi_{c2}}{v_1 + v_2}. \tag{29}$$

C. Motional Conductance Matrix and Gain Condition

In the simplified small-phase-shift case discussed in (29), if ϕ_{c1} and ϕ_{c2} are both set to zero, simply $\phi_R = -\pi/2$ is obtained. This greatly simplifies equation pair (21) to $\phi_1 = \phi_2 = 0$ and the force equation (24), resulting in

$$F(t) = -\kappa v_B (v_1 + v_2)\cos(\omega_R t). \tag{30}$$

This phase assumption also provides a simplification for equation set (17) to

$$\begin{aligned} i_1(t) &= \omega_1 \gamma (v_1 + v_2)\cdot\cos(\omega_1 t) \\ i_2(t) &= \omega_2 \gamma (v_1 + v_2)\cdot\cos(\omega_2 t) \end{aligned} \tag{31}$$

and corresponding $v_{\mathrm{drive},1}(t)$ and $v_{\mathrm{drive},2}(t)$ can be obtained from (20)

$$\begin{aligned} v_{\mathrm{drive},1}(t) &= v_1\cos(\omega_1 t) = R_{\mathrm{amp}}\cdot i_1(t) \\ v_{\mathrm{drive},2}(t) &= v_2\cos(\omega_2 t) = R_{\mathrm{amp}}\cdot i_2(t) \end{aligned} \tag{32}$$

where the transimpedance gain of the circuit R_{amp} at both frequencies is also assumed to be equal. Unlike the open-loop analysis, both drive voltages exist simultaneously in the oscillator since both currents appear simultaneously as well. Equation (30) indicates that the effects of the two drive voltages are simply additive, even though we are dealing with a nonlinear system.

The aforementioned expressions provide a path in determining the relative amplitudes of the two signals

$$\frac{i_1}{i_2} = \frac{v_1}{v_2} = \frac{\omega_1}{\omega_2}. \tag{33}$$

One also notices a form of cross mixing of inputs and outputs occurring within the device, which may be expressed compactly as

$$\begin{bmatrix} i_1 \\ i_2 \end{bmatrix} = G_{\mathrm{resonator}} \begin{bmatrix} v_1 \\ v_2 \end{bmatrix} \tag{34}$$

where $G_{\mathrm{resonator}}$ is the motional conductance of the resonator, which is now a 2×2 matrix

$$G_{\mathrm{resonator}} = \gamma \begin{bmatrix} \omega_1 & \omega_1 \\ \omega_2 & \omega_2 \end{bmatrix}. \tag{35}$$

This matrix form of $G_{\mathrm{resonator}}$ enables either of the two input voltages to contribute to both the output currents. The conductances $\gamma\omega_1$ and $\gamma\omega_2$ are directly observable through the network analyzer as described by equation pair (18). Meanwhile, equation pair (32) may also be expressed in matrix form as

$$\begin{bmatrix} v_1 \\ v_2 \end{bmatrix} = R_{\mathrm{amp}} \begin{bmatrix} i_1 \\ i_2 \end{bmatrix} \tag{36}$$

following which the algebraic manipulation of (34)–(36) gives us the required amplifier gain

$$R_{\mathrm{amp}} = \frac{1}{\gamma(\omega_1 + \omega_2)} = \frac{1}{2\gamma\omega_R}. \tag{37}$$

Note that this required gain is double the dc motional resistance presented in (19) ($\omega_R \approx \omega_{\mathrm{Res}}$). This is a useful result as it implies that no change in the oscillator gain is required in converting from dc polarization to ac polarization, as long as the rms value of the polarization $v_p(t)$ in the ac case (which is $v_B/\sqrt{2}$) equals the dc polarization voltage (simply v_B) in the dc case.

D. Modulation Artifacts

As the polarization voltage $v_p(t)$ varies sinusoidally, the electrostatic spring-softening effect causes periodic modulation of the frequency ω_{Res}. Since the softening is known to be a squared function of the polarization voltage, the modulation occurs at $2 \times \omega_B$. The spring-softening effect is inversely related to the stiffness of the mechanical spring in the system, so this frequency-modulation (FM) effect should be reduced in high-stiffness bulk-mode resonators.

In addition, the closed-loop drive force (23) is not a simple sinusoid but is composed of three dominant excitation frequencies. Under the linear resonator model, some mechanical excitation at the additional $(\omega_R \pm 2\omega_B)$ forcing frequencies is expected. A high-quality-factor resonator should easily reduce these amplitude-modulation (AM) effects.

Oscillators typically have a gain controller that actively adjusts the amplifier gain so that oscillations are sustained. Since the output signal from the resonator is composed of two sinusoids, the envelope of the output signal shows a "beat" at ω_B, and the envelope of output power shows a variation at $2 \times \omega_B$. This envelope can be misread by the gain controller as a variation in the output power, and it may actively attempt to adjust for the variations. Although the gain controller can be designed with a very low bandwidth, small attempts to

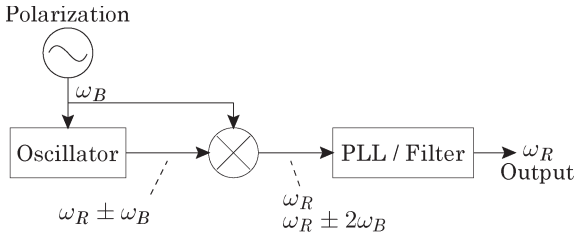

Fig. 7. Proposed oscillator topology with an external polarization source. The mixer and filter help generate a single-tone output that is independent of ω_B.

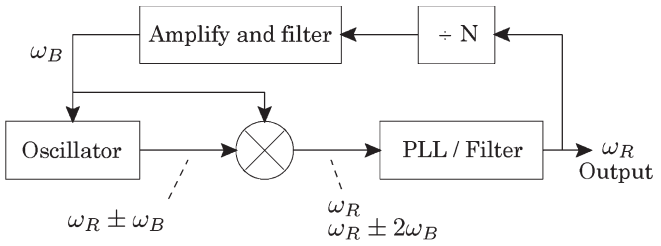

Fig. 8. Oscillator topology modified from Fig. 7 for internal/bootstrapped polarization to remove the dependence on an external polarization oscillator.

adjust the periodically changing envelope lead to a periodically changing amplifier gain. This creates additional AM.

Both these AM and FM effects occur at $2 \times \omega_B$ and consequently overlap in the spectral domain. Electrically, these artifacts are visible in the output spectrum of the oscillator, positioned $2 \times \omega_B$ away from the dominant output tones in Fig. 6. Additional artifacts can appear due to frequency intermodulation through amplifier nonlinearities.

V. Signal Conditioning for Single-Tone Output

A. External AC Polarization Source

The power spectrum of the oscillator previously described primarily shows two peaks at $\omega_R - \omega_B$ and $\omega_R + \omega_B$ (i.e., ω_1 and ω_2). However, in a directly usable frequency reference, the output frequency should ideally be a single-tone sinusoid at the resonator frequency ω_R, and the dependence on the external polarization frequency ω_B must be removed.

The generation of a single-tone output signal has been previously explained in [14]. As shown in Fig. 7, the oscillator output is mixed with the polarization signal to regenerate a dominant tone at the mechanical resonance frequency ω_R. However, this mixed signal includes many spurs at multiples of the bias frequency around the ω_R carrier. These spurs can be eliminated by placing a narrow-band filter at the frequency ω_R. As described in [14], a phase-locked loop (PLL) was used to perform this filtering task. The output signal from the PLL's voltage-controlled oscillator (VCO) is a 0–5-V square waveform, which can then be used as a frequency reference.

In the case of a PLL-based filter, the loop filter component helps determine the overall filter bandwidth. Choosing a narrow bandwidth loop filter eliminates the modulation artifacts and other noise sources present in the spectrum that are away from ω_R. However, using a wider bandwidth loop filter enables the VCO output phase noise to follow the oscillator's phase noise. These two tradeoffs regarding loop filter selection can be resolved by using higher polarization frequency ω_B (which can be facilitated by higher frequency resonators). Doing so moves the spurious frequency content further away from ω_R, such that a higher bandwidth loop filter still achieves sufficient sideband reduction, while allowing the VCO to follow the oscillator-defined phase noise.

Since, after filtering, the AM and FM sidebands (see Section IV-D) are significantly attenuated, very little modulation is expected at the output.

B. Internal AC Polarization Source

The previously described oscillator topology provides a method to build a drift-free temperature-compensated oscillator. However, it requires the existence of an additional oscillator to generate the polarization source frequency ω_B. Since an additional oscillator may not be affordable in many cases and indeed could be a handicap for certain practical stand-alone systems, we propose the following bootstrapping methodology (shown in Fig. 8).

The VCO in the PLL generates a square wave at all times, irrespective of having a successful frequency lock to any input signal. When the MEMS oscillator is not started, there is no input signal to the PLL, and the VCO signal has a very noisy and arbitrary frequency. This output square wave, however, can be used to generate a lower frequency polarization signal using a digital divide-by-N, followed by amplification and filtering circuitry. This new lower frequency signal feeds the resonator, which then allows the oscillator to start up. Once the oscillator is started, the PLL can obtain the lock, and the VCO output frequency changes. This change in the VCO frequency does not have an effect on the dominant tone at the PLL input, since that is always generated at ω_R after the mixer.

VI. Frequency-Stability Results

The device that was chosen for testing the fully ac oscillator methods has previously demonstrated very large drifts [5] under dc polarization. This is a double-ended tuning fork resonator with 0.42 μm of wet thermal SiO_2 and has a resonance frequency of about 1.077 MHz. All testing was performed in a temperature-controlled chamber at 40 °C. The device is sealed at the wafer level using "epi-seal" encapsulation [19]. Resonators built with the "epi-seal" encapsulation technology, in its oxide-free version, have previously demonstrated excellent frequency stability over very long periods of time [20].

A. External DC Polarization

The resonator was first tested under dc polarization with a conventional oscillator (the circuit discussed in [18]) to check for the familiar frequency drifts that were previously identified in [5]. As shown in Fig. 9, the oscillator frequency immediately moves away from the starting frequency and appears to be making a very slow approach to some eventual steady-state value with a very large time constant. In this case, about −90-ppm drift is observed in 42.5 h. It has been previously determined that these transients in frequency are due to mobile charge [5].

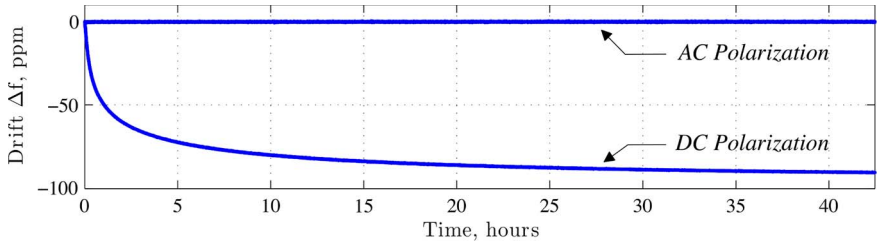

Fig. 9. Example of the large frequency drift in a 1.077-MHz SiO_2-coated resonator under dc polarization. The result of (external) ac polarization on the same device is also presented here, exhibiting the significant improvement in performance. Both data sets are normalized to their respective start frequency. The complete ac polarization data set used for this figure is shown in Fig. 11.

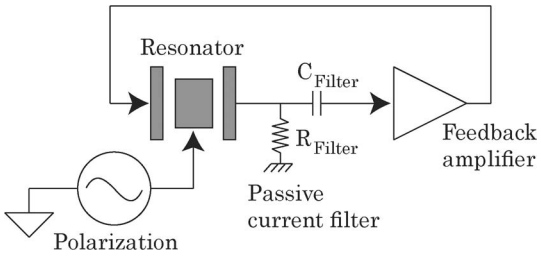

Fig. 10. Schematic of the modified oscillator used in ac polarization testing. A high-pass current filter ($R_{\mathrm{Filter}} = 3.3$ kΩ, $C_{\mathrm{Filter}} = 100$ pF, and 480-kHz cutoff frequency) between the resonator output and the feedback amplifier permits high-frequency currents to pass to the amplifier, while attenuating low-frequency currents such as the polarization feedthrough (14).

These transients reappear when the oscillator is turned off and on or when the dc polarization potential is changed.

B. External AC Polarization

The oscillator used for the dc experiments was subsequently slightly modified with a passive first-order current filter (see Fig. 10) to reduce the large polarization feedthrough current [identified in equation set (14)]. The mixer and PLL were also added after the oscillator, as shown in Fig. 7. As a result, the same device was tested with the same physical oscillator circuit (operational amplifiers and passives). The PLL was implemented with a first-order loop filter and a Texas Instruments 4046 PLL integrated circuit (IC) on a custom printed circuit board.

The test was performed for over 500 h (21 d), and very good stability was observed (see Fig. 11). The large long-time-constant drift in frequency is no longer present. A linear fit to the data exposes a 0.15-ppm/week drift trend that is otherwise lost within the variance around the average frequency. The data shown in this figure complement the short-duration (40 h) data set shown in [14] with a higher stability and longer duration result, increasing our confidence in the efficacy of this system.

C. Internal AC Polarization

A basic system was assembled to demonstrate the method discussed in Section V-B. We used a digital-counter-based divider on a prototyping breadboard, followed by a Krohn-Hite model 3750 filter (Krohn-Hite Corporation, Brockton, MA) and a custom-built audio amplifier (National Semiconductor LME49811). The gain of the audio amplifier was found to drift over time, which changed the amplitude of the generated polarization voltage. A simple gain controller was incorporated to improve the amplitude stability of this source.

The result of long-duration stability testing of this system over 380 h is shown in Fig. 12. Again, we see that the large long-time-constant drift is no longer present. The exact source of the very small residual drift (linear fit indicates about +1.3-ppm total drift or 0.57 ppm/week) is still under investigation. We suspect that the amplification and filtering electronics in the polarization generation path are responsible for this residual drift.

The variance in the raw frequency data in Fig. 12 is noticeably larger than that in Fig. 11. This difference might be attributed to distortion from the audio amplifier that was used in the polarization feedback path (the polarization signal output from the amplifier is visibly distorted) or to a slight modification to the PLL filter parameters that occurred between these two experiments.

VII. Conclusion

MEMS often incorporate various dielectrics to take advantage of their mechanical and electronic properties. However, these devices are known to occasionally show problems that stem from charge trapping and charge movement on surfaces and within the bulk of the dielectric material. In this paper, we have discussed how ac polarization, with zero dc, can circumvent these charging issues for electrostatically transduced resonant MEMS. Furthermore, we have presented the mathematical theory behind open-loop probing, as well as closed-loop oscillator operation, for ac-polarized resonators. Although, under ac polarization, multiple frequencies participate in the system, the devices still operate under the basic assumptions of linearity. This paper has also supported the stated theoretical arguments with experimental data, showing the successful operation of self-sustaining oscillators.

Although much work still needs to be performed on predicting and characterizing the phase noise performance of these oscillators, it has been observed [21] that these oscillators are no longer sensitive to low-frequency noise. Instead, it is the noise in the ac polarization source that is most relevant in this case. Even though the demonstrated experimental oscillators are not optimized for noise performance, we have observed significant improvements in frequency stability of drift-susceptible SiO_2-coated resonators over long periods of time. Despite some additional overhead required in realizing the proposed systems, the additional electronics should be possible to implement

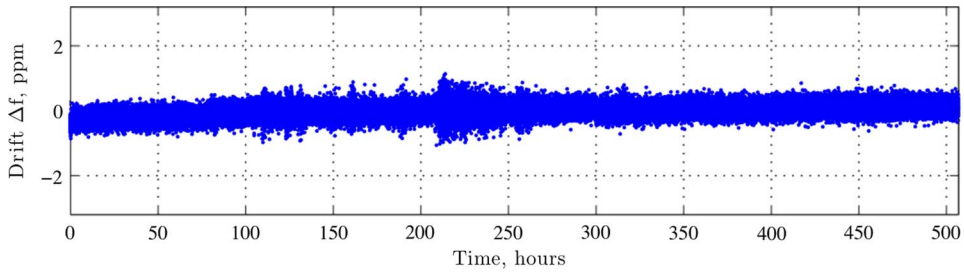

Fig. 11. Long-term observation of output frequency measured using a counter, for the oscillator topology from Fig. 7. This test was performed on the same SiO_2-coated device that was used with dc polarization in Fig. 9, with the same physical oscillator circuit. Note that the very large frequency drift is no longer present, even though the same charge-susceptible resonator is used.

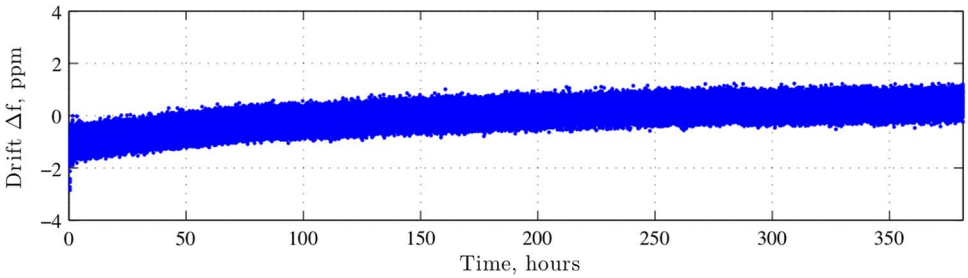

Fig. 12. Long-term observation of output frequency measured using a counter, for the oscillator topology from Fig. 8. Again, this test was performed on the same SiO_2-coated device that was used with dc polarization in Fig. 9, with the same physical oscillator circuit board. Although the very large frequency drift is no longer present, there is a very small residual drift in the frequency.

on application-specific ICs. The generalized methodology described in this paper can be applied to other systems to realize improvements of long-term stability with respect to charge drift.

ACKNOWLEDGMENT

This work was performed at Stanford University and the Center on Interfacial Engineering for Microelectromechanical Systems. The authors would like to thank Dr. S. A. Chandorkar and Dr. M. A. Hopcroft for their assistance in fabrication; H. Lee, S. Yoneoka, and Dr. I. Bargatin of Stanford University, Prof. A. Seshia of Cambridge University, and Prof. R. Bahl of the Indian Institute of Technology Delhi for the many enlightening discussions and feedback that the authors received; and Prof. C. Nguyen, Prof. A. Lal, and Prof. A. Shkel of the Defense Advanced Research Projects Agency for their guidance and support. The authors would also like to thank Prof. S. Senturia of the Massachusetts Institute of Technology for the initial encouragement to investigate ac polarization in resonators.

REFERENCES

[1] G. Fedder, S. Santhanam, M. Reed, S. Eagle, D. Guillou, M. Lu, and L. Carley, "Laminated high-aspect-ratio microstructures in a conventional CMOS process," *Sens. Actuators A, Phys.*, vol. 57, no. 2, pp. 103–110, Jan. 1996.

[2] P. R. Scheeper, W. Olthuis, and P. Bergveld, "A silicon condenser microphone with a silicon nitride diaphragm and backplate," *J. Micromech. Microeng.*, vol. 2, no. 3, pp. 187–189, Sep. 1992.

[3] D. Weinstein and S. Bhave, "Internal dielectric transduction in bulk-mode resonators," *J. Microelectromech. Syst.*, vol. 18, no. 6, pp. 1401–1408, Dec. 2009.

[4] M. Ziaei-Moayyed, E. P. Quevy, J. Hsieh, and R. T. Howe, "Efficient internal electrostatic transduction of the 41st radial mode of a ring resonator," in *Proc. IEEE Int. Conf. Microelectromech. Syst.*, Hong Kong, Jan. 24–28, 2010, pp. 711–714.

[5] G. Bahl, R. Melamud, B. Kim, S. Chandorkar, J. Salvia, M. Hopcroft, D. Elata, R. Hennessy, R. Candler, R. Howe, and T. Kenny, "Model and observations of dielectric charge in thermally oxidized silicon resonators," *J. Microelectromech. Syst.*, vol. 19, no. 1, pp. 162–174, Feb. 2010.

[6] J. Wibbeler, G. Pfeifer, and M. Hietschold, "Parasitic charging of dielectric surfaces in capacitive microelectromechanical systems (MEMS)," *Sens. Actuators A, Phys.*, vol. 71, no. 1/2, pp. 74–80, Nov. 1998.

[7] K. Frederick and G. Fedder, "Mechanical effects of fatigue and charge on CMOS MEMS," *Proc. SPIE*, vol. 4180, pp. 108–116, 2000.

[8] S. Kalicinski, H. Tilmans, M. Wevers, and I. D. Wolf, "A new characterization method for electrostatically actuated resonant MEMS: Determination of the mechanical resonance frequency, quality factor and dielectric charging," *Sens. Actuators A, Phys.*, vol. 154, no. 2, pp. 304–315, Sep. 2009.

[9] C. Goldsmith, J. Ehmke, A. Malczewski, B. Pillans, S. Eshelman, Z. Yao, J. Brank, M. Eberly, R. Co, and T. Dallas, "Lifetime characterization of capacitive RF MEMS switches," in *Proc. IEEE MTT-S Int. Microw. Symp. Dig.*, 2001, vol. 1, pp. 227–230.

[10] H. Chandrahalim, S. Bhave, E. Quevy, and R. Howe, "Aqueous transduction of poly-SiGe disk resonators," in *Proc. Transducers*, 2007, pp. 10–14.

[11] T. Sounart and T. Michalske, "Electrostatic actuation without electrolysis in microfluidic MEMS," in *Proc. Transducers*, Jun. 2003, pp. 615–618.

[12] V. Mukundan and B. Pruitt, "MEMS electrostatic actuation in conducting biological media," *J. Microelectromech. Syst.*, vol. 18, no. 2, pp. 405–413, Apr. 2009.

[13] Z. Peng, X. Yuan, J. Hwang, D. Forehand, and C. Goldsmith, "Superposition model for dielectric charging of RF MEMS capacitive switches under bipolar control-voltage waveforms," *IEEE Trans. Microw. Theory Tech.*, vol. 55, no. 12, pp. 2911–2918, Dec. 2007.

[14] G. Bahl, J. Salvia, I. Bargatin, S. Yoneoka, R. Melamud, B. Kim, S. Chandorkar, M. Hopcroft, R. Bahl, R. Howe, and T. Kenny, "Charge-drift elimination in resonant electrostatic MEMS," in *Proc. IEEE Int. Conf. Microelectromech. Syst.*, Hong Kong, Jan. 24–28, 2010, pp. 108–111.

[15] R. Melamud, S. A. Chandorkar, B. Kim, H. K. Lee, J. Salvia, G. Bahl, M. A. Hopcroft, and T. W. Kenny, "Temperature insensitive composite micromechanical resonators," *J. Microelectromech. Syst.*, vol. 18, no. 6, pp. 1409–1419, Dec. 2009.

[16] A. Wong and C. Nguyen, "Micromechanical mixer-filters ("mixler")," *J. Microelectromech. Syst.*, vol. 13, no. 1, pp. 100–112, Jan. 2004.

[17] B. Bahreyni and C. Shafai, "Oscillator and frequency-shift measurement circuit topologies for micromachined resonant devices," *Sens. Actuators A, Phys.*, vol. 137, no. 1, pp. 74–80, Jun. 2007.

[18] J. Salvia, R. Melamud, S. A. Chandorkar, S. F. Lord, and T. W. Kenny, "Real-time temperature compensation of MEMS oscillators using an

integrated micro-oven and a phase lock loop," *J. Microelectromech. Syst.*, vol. 19, no. 1, pp. 192–201, Feb. 2010.

[19] R. Candler, M. Hopcroft, B. Kim, W. Park, R. Melamud, M. Agarwal, G. Yama, A. Partridge, M. Lutz, and T. Kenny, "Long-term and accelerated life testing of a novel single-wafer vacuum encapsulation for MEMS resonators," *J. Microelectromech. Syst.*, vol. 15, no. 6, pp. 1446–1456, Dec. 2006.

[20] B. Kim, R. Candler, M. Hopcroft, M. Agarwal, W. Park, and T. Kenny, "Frequency stability of wafer-scale film encapsulated silicon based MEMS resonators," *Sens. Actuators A, Phys.*, vol. 136, no. 1, pp. 125–131, May 2007.

[21] G. Bahl, J. Salvia, H. K. Lee, R. Melamud, B. Kim, R. Howe, and T. Kenny, "Heterodyned electrostatic transduction oscillators evade low frequency noise aliasing," in *Proc. Solid-State Sens., Actuators Microsyst. Workshop*, Hilton Head Island, SC, Jun. 6–10, 2010, pp. 384–385.

Gaurav Bahl (M'10) received the B.Eng. degree in electrical engineering from McMaster University, Hamilton, ON, Canada, in 2005, and the M.S. degree and the Ph.D. degree in electrical engineering from Stanford University, Stanford, CA, in 2008 and 2010, respectively. His work at Stanford University focused on studying dielectric charging in microelectromechanical systems and drift stability of encapsulated silicon microresonators.

In 2008, he was with HP Laboratories, Palo Alto, CA, where he published on circumventing charging-related drift issues within the dielectrics of surface electrode actuators. He is currently a Postdoctoral Research Fellow at the University of Michigan, Ann Arbor, where he is developing optomechanical oscillators for frequency reference applications.

Dr. Bahl was a recipient of the Ontario Professional Engineers Foundation for Education Gold Medal in 2005.

James C. Salvia (S'03–M'10) received the B.S. degree in electrical and computer engineering from Carnegie Mellon University (CMU), Pittsburgh, PA, and the M.S. and Ph.D. degrees in electrical engineering from Stanford University, Stanford, CA, in 2008 and 2010, respectively. His work at Stanford University focused on circuit development for the stabilization and control of microresonator-based oscillators.

He was a Research Assistant with CMU, where he developed on-chip magnetic inductors for high-frequency applications. He was an Intern with the Bettis Atomic Power Laboratory, Robert Bosch Corporation, and Atheros Communications. He is currently a Mixed Signal Design Engineer with SiTime Corporation, Sunnyvale, CA.

Renata Melamud (M'09) received the B.S. degree (with honors) in mechanical engineering from Carnegie Mellon University, Pittsburgh, PA, in 2003, and the M.S. and Ph.D. degrees in mechanical engineering from Stanford University, Stanford, CA, in 2006 and 2009, respectively. Her dissertation, *Temperature Insensitive Micromechanical Resonators*, concerned the passive temperature compensation of silicon resonators for frequency references.

She is currently a MEMS Development Engineer with SiTime Corporation, Sunnyvale, CA, where she is developing the next-generation microelectromechanical systems resonators for timing references.

Dr. Melamud was recognized as an Andrew Carnegie Scholar at Carnegie Mellon University and as a Gabilan Stanford Graduate Fellow at Stanford University.

Bongsang Kim (S'06–M'08) received the B.S. degree in mechanical design and production engineering from Seoul National University, Seoul, Korea, and the M.S. and Ph.D. degrees in mechanical engineering with an electrical engineering minor from Stanford University, Stanford, CA, in 2004 and 2007, respectively.

From 1998 to 2001, he was a Mechanical Engineer with Hyundai. In 2005, he was an Intern with Agilent Labs, where he worked on the development of nanosteppers that are capable of 1000-g acceleration. He was a Postdoctoral Researcher with the Berkeley Sensor and Actuator Center (BSAC), University of California, Berkeley, where he was working with Prof. Clark Nguyen. He is currently with Sandia National Laboratories, Alberquerque, NM. His research interests include RF microelectromechanical systems (MEMS), reliability of micro/nanoscale structures, MEMS packaging, material diffusion, and energy loss and stability of micromechanical resonators.

Dr. Kim was a recipient of the Best Student Award at the IEEE Frequency Control Symposium 2007 and the Best Paper Award at the 2008 BSAC Industrial Advisory Board fall meeting.

Roger T. Howe (S'80–M'84–SM'93–F'96) received the B.S. degree in physics from Harvey Mudd College, Claremont, CA, and the M.S. and Ph.D. degrees in electrical engineering from the University of California, Berkeley (UC Berkeley), in 1981 and 1984, respectively.

From 1984 to 1987, he was a Faculty Member at Carnegie Mellon University, Pittsburgh, PA, and at the Massachusetts Institute of Technology, Cambridge. After that, he was a Professor at UC Berkeley until 2005. He is currently the William E. Ayer Professor in the Electrical Engineering Department, Stanford University, Stanford, CA. His research interests include MEMS design, micro- and nanomachining processes, and parallel assembly processes. A focus of his research has been on processes to fabricate integrated microsystems, which incorporate both silicon-integrated circuits and MEMS. He has made contributions to the design of MEMS accelerometers, gyroscopes, electrostatic actuators, and microresonators. He is a Cofounder of Silicon Clocks, Inc., a start-up company commercializing integrated MEMS resonator-based timing products.

Prof. Howe was a Cogeneral Chair of the 1990 IEEE MEMS Workshop in Napa, CA, and the Technical Program Chair of Transducers '03 in Boston, MA. He is an Editor of the JOURNAL OF MICROELECTROMECHANICAL SYSTEMS. He was a corecipient of the 1998 IEEE Cledo Brunetti Award and was elected to the U.S. National Academy of Engineering in 2005 for his contributions to MEMS processes, devices, and systems.

Thomas W. Kenny (M'10) received the B.S. degree in physics from the University of Minnesota, Minneapolis, in 1983, and the M.S. and Ph.D. degrees in physics from the University of California, Berkeley, in 1987 and 1989, respectively.

From 1989 to 1993, he was with the National Aeronautics and Space Administration Jet Propulsion Laboratory, Pasadena, CA, where his research focused on the development of electron-tunneling high-resolution microsensors. Since 1994, he has been with the Mechanical Engineering Department, Stanford University, Stanford, CA, where he directs MEMS-based research in a variety of areas, including resonators, wafer-scale packaging, cantilever beam force sensors, microfluidics, and novel fabrication techniques for micromechanical structures. From 2006 to 2010, he was a Program Manager with the Microsystems Technology Office, Defense Advanced Research Projects Agency, where he started and managed programs in thermal management (TGP, MACE, NTI, and MCM), nanomanufacturing (TBN), manipulation of Casimir forces (CEE), and the Young Faculty Award. He is the Founder and Chief Technical Officer of Cooligy, Inc., Mountain View, CA, a microfluidics chip cooling component manufacturer, and also the Founder and a Board Member of SiTime Corporation, Sunnyvale, CA, a developer of CMOS timing references using MEMS resonators. He has authored or coauthored over 200 scientific papers and is the holder of 44 issued patents.

Dr. Kenny is currently the Stanford Bosch Faculty Development Scholar and was the General Chairman of the 2006 Hilton Head Solid State Sensor, Actuator, and Microsystems Workshop.